Uniform TiO_2 and Al_2O_3 coated meltblown nonwoven fabrics for photocatalytic drinking water treatment via atomic layer deposition

Alexander G. Aragon[†§], Jaime A. Cardenas Sanchez[‡§], Carlos Zimeri[¶], Eunkyoung Shim[¶], Xiaomeng Fang[¶], and Kyana R. L. Young[§*]

[†]Department of Chemistry, Wake Forest University, 1834 Wake Forest Road, Winston-Salem, NC, 27109, USA.

[‡]Department of Biology, Wake Forest University, 1834 Wake Forest Road, Winston-Salem, NC, 27109, USA.

[§]Department of Engineering, Wake Forest University, 455 Vine Street, Winston-Salem, NC, 27101, USA.

[¶]Department of Textile Engineering, Chemistry and Science, North Carolina State University, 1020 Main Campus Drive, Raleigh NC, 27606, USA.

[*]Corresponding author.

Email address: youngk@wfu.edu (K. R. L. Young)

Abstract

Within the field of photocatalytic drinking water treatment, the controlled manufacturing of semiconductor catalysts with high surface area is crucial for their development and commercialization. Atomic layer deposition (ALD) allows a high degree of control and uniformity for the deposition of semiconductor films and can be done with minimal waste and mild toxicity. In this study, we compare TiO_2 and Al_2O_3 as catalyst layers deposited via ALD on three meltblown nonwoven fabrics manufactured from polypropylene and one commercially

available textile from Laprotex™ for the inactivation of *Escherichia coli* (*E. coli*). It is observed that in the presence of an ultraviolet light emitting diode (UV-LED) light source (255 nm), 1.35 log *E. coli* inactivation is achieved. However, in the presence of catalyst coated meltblown nonwoven fabrics > 4 log *E. coli* inactivation is observed suggesting a much higher rate of hydroxyl radical formation on the catalyst surface leading to cell death.

Keywords: Antimicrobial, Nonwovens, Drinking water, Atomic layer deposition, Photocatalysis

1. Introduction

Water is an essential natural resource, and perhaps the greatest need of humanity for health, wellbeing, development, and sustenance of life [1,2]. Unfortunately, 20% of the world's population has no access to clean drinking water, and this is further complicated with the growing world population in recent years [3,4]. Many types of water contaminants exist such as chemical waste, heavy metals, and biological agents such as disease-causing microbes. In most cases where clean water is inaccessible, the greatest concern is disease such as cholera, typhus, polio, tuberculosis, diphtheria and diarrhea [5]. One such microbe that signals issues with water quality is *Escherichia coli* (*E. coli*). *E. coli* serves as an indicator microbe to verify the presence of fecal indicator organisms, and thus serves as a good model for testing disinfection methods. It is crucial to develop drinking water treatment methods that inactivate these organisms in both a safe and sustainable way and utilizing *E. coli* as a model allows for ease of testing.

Several conventional drinking water disinfection methods such as chlorination, ozonation, radiation, advanced filtration and the use of ultraviolet (UV) light have been used over the years for such treatment [2,6]. However, there are several key drawbacks suffered by these conventional methods such as the formation of disinfection byproducts which are potentially

toxic/carcinogenic, high operational and maintenance cost, the development of antibiotic drug resistance over time, and low disinfection efficiency [2,3,5,7,8]. Conventional disinfection technologies are also met with implementation challenges and thus alternative methods must be sought to achieve truly sustainable, low cost, and minimally toxic water treatment methods. Photocatalytic disinfection remains an innovative and promising option with high disinfection potential for water purification [3,9]. Given the minimal operational cost, and highly sustainable nature of photocatalysis, the development of catalysts utilized for this type of disinfection is a current area of research with high interest [4].

Traditional photocatalysis is focused on the utilization of semiconductor materials such as metal oxides [10–12], perovskite oxides [13,14], and metal chalcogenides [10,15] all synthesized chemically with the use of potentially toxic reagents. These catalysts also typically are produced in bulk powders, or thin films where surface area and reproducibility concerns arise in terms of large-scale water treatment usage. Therefore, it is crucial to develop methods to produce semiconductor photocatalysts with high uniformity, minimal toxicity, and high surface area for industrial use. ALD provides strong levels of controllability, and uniformity to produce such semiconductor photocatalysts including TiO_2 and Al_2O_3 which are utilized in this study. To date, metal oxides such as TiO_2 and Al_2O_3 have been heavily studied as antibacterial agents prepared via traditional chemical methods [16,17], and the preparation of these metal oxides via ALD shows promise for the large-scale production of photocatalysts for drinking water treatment.

In this study, nano TiO_2 and Al_2O_3 was attached to the surface of meltblown nonwoven fabrics via ALD methods to prepare a photocatalyst for the inactivation of *E. coli* in water. Textiles have been shown to also be useful for antimicrobial treatment [18,19] and thus can be seen as a strong substrate choice for the preparation of photocatalytic disinfection technologies based on ALD.

Due to the near zero waste of raw materials and environmental pollution, ALD proves to be a high value synthetic process for the development of antibacterial textiles [19,20]. The overall structural properties of thin films on meltblown nonwoven fabrics are discussed to understand the deposition process and confirm uniform synthesis of TiO_2 and Al_2O_3 on the surface. The photocatalytic antibacterial activity of catalyst coated meltblown nonwoven fabrics is discussed and compared from each metal oxide, and a UV-LED light source. Lastly, the overall stability of the catalyst films is discussed with respect to reusability.

2. Experimental

2.1. Materials

Titanium (IV) isopropoxide (99.995%) as a precursor of titanium was acquired from Thermo Fisher. Trimethlyaluminum (TMA, 97%) as a precursor of aluminum was acquired from Sigma Aldrich. Ultrapure deionized water (Mili-Q) was utilized as an oxygen source for ALD. Metocene 650W Polypropylene (PP) (LyondellBasell, Netherlands) with a 500 g/10 min melt flow rate (MFR) and 0.91 g/cm^3 density was used as the raw material for the production of the meltblown nonwoven fabrics.

2.2. Bacterial Stock Preparation

E. coli was used as the model bacteria microbial contaminant to assess the inactivation efficacy of the ALD photocatalyst on the meltblown nonwoven fabric. *E. coli* BA-1883 (American Type Culture Collection, USA) was aseptically transferred to Nutrient Broth (Difco™, USA) and placed in an incubator at 37°C for 5 hours. The bacterial growth was then centrifuged at 2000 rpm for 2 minutes, with the supernatant being disposed, and fresh phosphate buffered saline (PBS) added to resuspend the pellet. The pellet and PBS mixture were vortexed and centrifuged

at 2000 rpm for 2 minutes; the supernatant was disposed, and fresh PBS was added bringing the *E. coli* stock concentration to 10^6 colony forming units (cfu) per milliliter.

2.3. Preparation of meltblown nonwoven fabrics

The meltblown nonwoven fabrics used in this study were produced using a pilot-scale Reicofil® (Reifenhauser, Germany) meltblown line equipped with a traditional Exxon style die (die orifice diameter = 400 μm, die orifice density = 35 holes/inch, setback = 1.2 mm, Total die width = 1.3 m) in the Nonwoven Institute at North Carolina State University (Raleigh, NC). Processing parameters were varied to control metlblown fabric structures and summarized in Table S1 (Supporting Information).

2.4. Synthesis of TiO_2 and Al_2O_3 films

The syntheses of TiO_2 and Al_2O_3 films were done via ALD methods utilizing an Arradiance GEMSTAR-6 benchtop chamber equipped with a furnace. Fabric samples along with a Si reference wafer were placed into the chamber and sequential deposition of Ti/Al and O were done chemically. For TiO_2, the deposition conditions included a chamber temperature of 150 ºC, Ti pulse time of 100 ms, followed by an N_2 purge of 23 s, and an O pulse time of 1000 ms followed by another N_2 purge of 28 s to complete a cycle. For Al_2O_3 these conditions were a chamber temperature of 125 ºC, Al pulse time of 22 ms, followed by a N_2 purge of 20 s, and an O pulse time of 22 ms followed by a N_2 purge of 28 s to complete a cycle. The growth rate for thin films was 0.03 nm/cycle for TiO_2 and 0.14 nm/cycle for Al_2O_3.

2.5. Characterization

The structural characteristics of thin films, and fabrics were examined using a scanning electron microscope (GEMINI300, Zeiss) paired with an energy dispersive X-ray spectrometer (Bruker)

for elemental analysis. A full detailed description of the characterization of the meltblown nonwoven fabric properties can be found in the Supporting Information. Determination of film thickness was done on a Si reference via XRR measurements performed on an X-ray diffractometer (D8 Discover, Bruker) equipped with Cu kα radiation and a Goebel mirror. Further characterization methods included IR spectroscopy (Spectrum 100, Perkin Elmer), and XPS spectroscopy (Escalab Xi+, Thermo Scientific). For the XPS experiment, avantage software was used to process the obtained data and combined Gaussian-Lorentz equations were used to fit curves of elements. The spectra charge correction is done using C1s binding energy of 284.8 eV.

2.6. Photocatalytic studies

2.6.1. Ultraviolet Light Emitting Diode Irradiation

For disinfection, a UV-LED (PearlBeam™, AquiSense Technologies) was used as a light source. The ILT-5000 radiometer, with SED 270/QT detector, was used for detection of irradiance (International Light Technologies, USA). For irradiance of the water sample, the reflection factor = 0.975, petri factor = 0.894, water factor = 0.981, and divergence factor = 0.975 were used to correct the irradiance values. The irradiance at the water surface is 0.041 mW/cm^2.

2.6.2. Experimental Conditions

An aliquot of 1.5 mL of the *E. coli* stock was added to 13.5 mL of Milli-Q water (25°C, 18.2Ω) in a glass 60 x 15 mm quartz Petri dish and placed on a magnetic stir plate to gently mix at 250 rpm. The Petri dish was placed under a collimated beam, where the UV-LED irradiated the sample at λ = 255 nm and was selected for its proximity to the peak absorbance (λ = 254 nm) responsible for DNA damage. Simultaneously, the meltblown nonwoven fabric was added to the Petri dish and the UV-LED was powered on. At the conclusion of irradiation, the meltblown

nonwoven fabric was then removed from the Petri dish and the solution was processed using the membrane filtration method (Standard Methods 9222B); the filter was placed on m-Endo Agar LES (Remel™, USA) in the incubator for 24 hours, at 37°C and then transferred to the EC Medium w/ MUG (Remel™, USA) for 4 hours at 44°C. After incubation, fluorescent colonies were quantified using the plate count method. The control groups were: Milli-Q (negative), bacteria stock solution (positive). The experimental groups were: meltblown nonwoven fabric, meltblown nonwoven fabric deposited with photocatalyst (TiO_2 or Al_2O_3), meltblown nonwoven fabric deposited with photocatalyst (TiO_2 or Al_2O_3) and UV-LED irradiated, Laprotex™, Laprotex™ deposited with photocatalyst (TiO_2 or Al_2O_3), Laprotex™ deposited with photocatalyst (TiO_2 or Al_2O_3) and UV-LED irradiated, photocatalyst (TiO_2 or Al_2O_3), photocatalyst (TiO_2 or Al_2O_3) irradiated with UV-LED, and UV-LED.

2.6.3. Inactivation kinetics

The log inactivation for the *E. coli* was determined using log inactivation calculation, where N_0 is the initial concentration of cfu/mL with no irradiation, N_f is the concentration of cfu/mL after UV-LED irradiation:

$$\log \frac{N_f}{N_0} = log\ inactivation \quad (1)$$

Comparison of log inactivation was conducted to assess the inactivation efficacy of the experimental conditions. Data for TiO_2 and Al_2O_3 was collected in triplicate and sextuplicate, respectively.

3. Results and Discussion

3.1. Thin film fabrication and structural properties

Thin films of TiO_2 and Al_2O_3 were deposited on the polypropylene based nonwovens via ALD and a full cycle of ALD is pictured in Scheme 1.

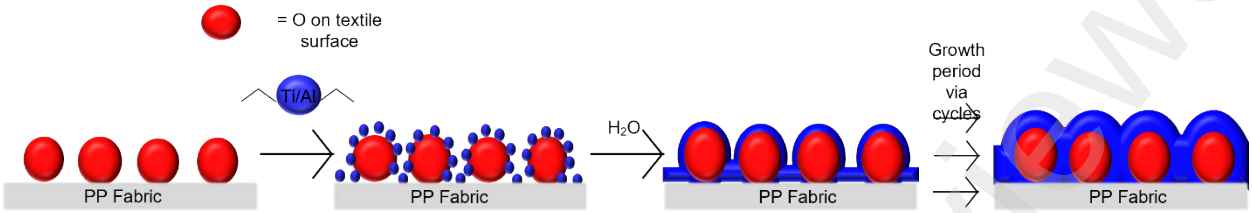

Scheme 1 : ALD deposition cycle on nonwoven fabric surface.

The Ti or Al precursor first react with hydroxyl groups on the surface of the meltblown nonwoven fabrics and the intermediate product then reacts with the water precursor to form a layer of TiO_2 or Al_2O_3 onto the surface. The thickness of these films can be adjusted via the number of ALD cycles run but for this work, an average film thickness of ~12 nm was utilized for the TiO_2 and Al_2O_3 films as determined via XRR experiments shown in Figure S1 (Supporting Information).

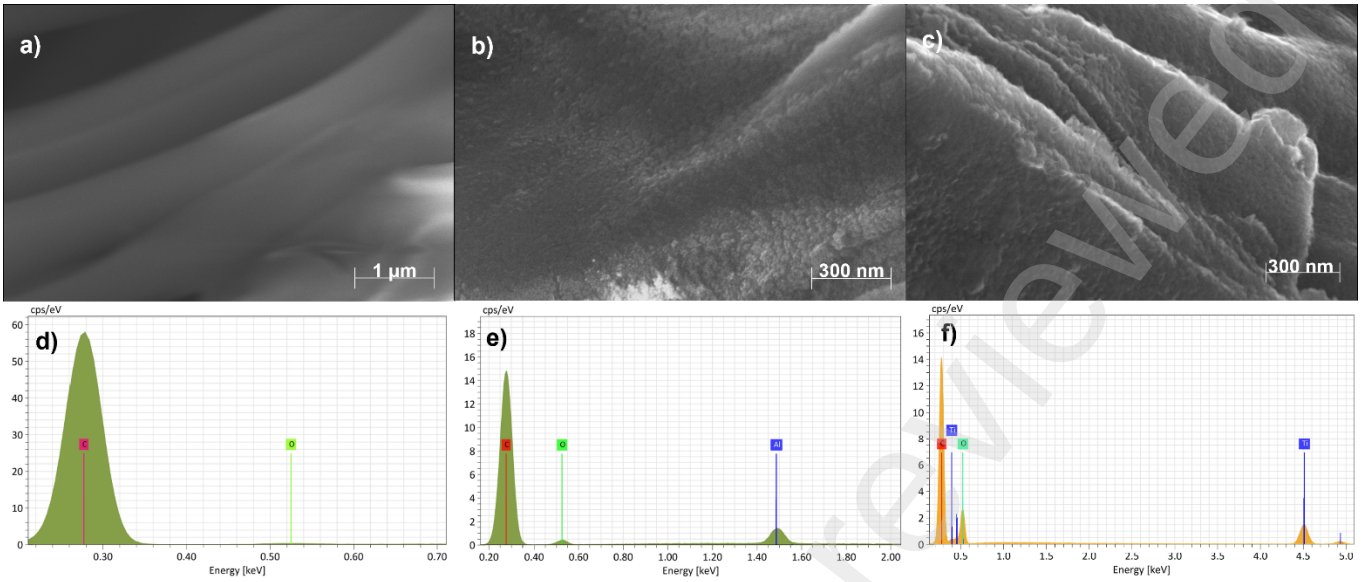

Figure 1: Structural morphology and elemental composition of pristine and treated nonwovens. a) SEM image of pristine fabric b) SEM image of Al_2O_3 coated fabric c) SEM image of TiO_2 coated fabric d) EDS spectrum of pristine fabric e) EDS spectrum of Al_2O_3 coated fabric f) EDS spectrum of TiO_2 coated fabric.

The morphology of ALD treated nonwovens compared to a pristine nonwoven fiber is shown in Figure 1a-c and was obtained via SEM imaging. An uneven surface of coating metal oxide coating is achieved after the ALD process when comparing the pristine fiber to Al_2O_3 and TiO_2 coated nonwovens respectively. The composition of the metal oxides as determined from EDS was found to be $Al_{1.42}O_{3.63}$ and $TiO_{4.3}$ and suggests oxygen rich films given the presence of oxygen in the bare nonwoven fabrics. The overall grain size of the deposited material varied with respect to the number of cycles (400 for TiO_2, 92 for Al_2O_3 respectively). EDS spectrum shown in Figure 1d-f paired with line scan data shown in Figure S2 and S3 (Supporting Information) suggest that the presence of Ti and Al on the surface of the meltblown nonwoven fabrics was achieved, and these elements were present in the same regions as oxygen on the surface. The morphology and elemental composition of ALD films deposited on the commercially available textile tested is shown in Figure S4 (Supporting Information).

To confirm successful deposition of TiO_2 and Al_2O_3 respectively on the surface of the meltblown nonwoven fabrics, both X-ray photoelectron spectroscopy (XPS) and IR spectroscopy were utilized to probe the chemical structure of the pristine and ALD treated meltblown nonwoven fabrics. The IR spectrum of treated and pristine nonwovens is shown in Figure 2a. The peaks at 2900, 1350, and 1053 cm^{-1} represent the stretch vibration of C-H, O-H, and C=C bonds respectively. After ALD treatment, a broad peak is present near 3500 cm^{-1} which represents the M-OH stretch vibration while the peak at 860 cm^{-1} is the Al-O-Al stretch suggesting that Al_2O_3

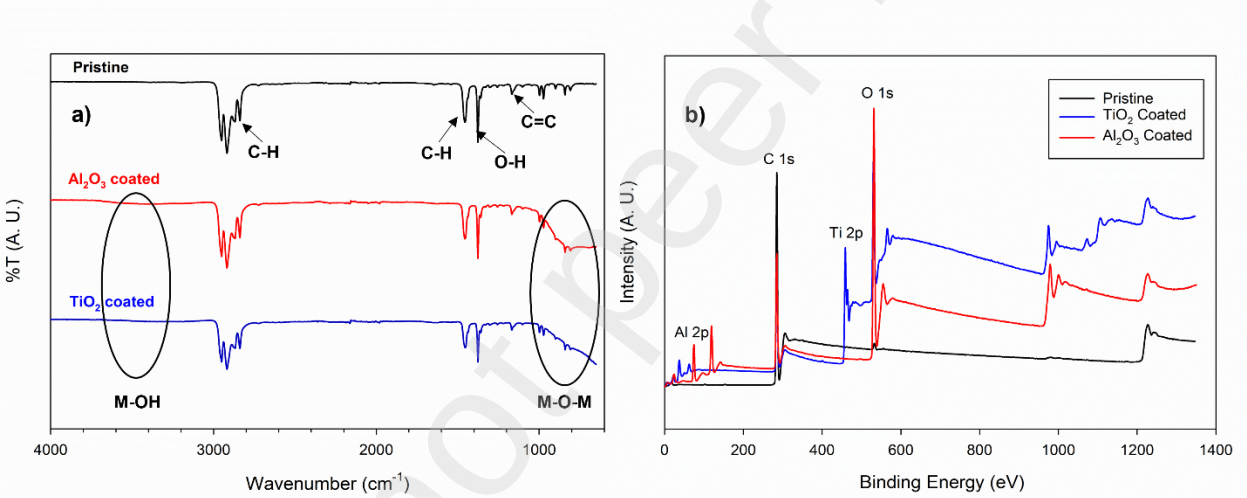

Figure 2: a) IR spectrum of pristine and ALD treated meltblown nonwoven fabrics b) XPS survey spectrum of pristine and ALD treated meltblown nonwoven fabrics.

was formed.

For TiO_2, the broad feature observed below 1000 cm^{-1} is the Ti-O-Ti stretch which also suggests deposition of TiO_2 on the surface. The C 1s and O 1s characteristic peaks appear at 284 and 532 eV respectively for the pristine nonwoven fabric as shown in the XPS survey spectrum in Figure 2b. When compared to the TiO_2 coated and Al_2O_3 coated meltblown nonwoven fabrics respectively, the presence of the characteristic Ti 2p and Al 2p peaks at 458 and 74 eV

respectively from the survey spectrum suggests the presence of Ti and Al respectively. This further supports the successful deposition of TiO_2 and Al_2O_3 on the meltblown nonwoven fabrics.

3.2. *E. coli* inactivation

In photocatalytic systems, the application of the external light provides the energy to move electrons to move from the valence band to the conduction band; this movement of electrons allows the production of the powerful oxidants in a bulk water system. The oxidant causes damage the DNA of waterborne microbes, thus rendering them inactive and unable to reproduce. The use of UV-LED, as an external light source, was analyzed as a singular treatment mechanism and compared to the similar treatment technologies that use light irradiated photocatalysts for disinfection practices.

Three nonwoven meltblown fabrics (PPW7, PPW8, and PPW9), a commercial (Laprotex™) fabric, and UV-LED were tested in a bulk water pH 7, temperature = 25°C, to assess the impact efficacy of inactivating *E. coli* using a collimated beam of UV-LED at λ = 255 nm (intensity = 0.041 mW/cm^2).

For experiments performed when the photocatalyst was deposited on the meltblown nonwoven fabric, inactivation of *E. coli* was evident (Figure 3). The PPW7, PPW8, and PPW9, deposited with AL_2O_3 and TiO_2, and a UV dose = 24.6 mJ/cm^2, achieved a minimum of 4.60 ± 0.21 and 5.00 ± 0.031 respectively. When exclusively irradiating the bulk water with UV-LED, UV dose = 24.6 mJ/cm^2, 1.35 ± 0.0422 log inactivation of *E. coli* was achieved (Table 1). The significant improvement in log *E. coli* inactivation for the coated meltblown nonwovens suggests high potential for the utilization of this technology as a multifunctional drinking water treatment option.

Table 1: Comparison of log inactivation for experimental types of *E. coli* inactivation.

Fabric Type	*Catalyst*	*External Light*	*Log Inactivation*
PPW7	Al_2O_3	UV-LED	4.90 ± 0.08
PPW8	Al_2O_3	UV-LED	4.60 ± 0.21
PPW9	Al_2O_3	UV-LED	4.60 ± 0.24
Larprotex™	Al_2O_3	UV-LED	4.80 ± 0.35
PPW7	TiO_2	UV-LED	4.40 ± 0.043
PPW8	TiO_2	UV-LED	4.40 ± 0.032
PPW9	TiO_2	UV-LED	4.40 ± 0.041
Laprotex™	TiO_2	UV-LED	5.00 ± 0.031
-	-	UV-LED	1.35 ± 0.0422

For the comparison of treatment efficacy between fabric type and TiO_2, the bacteria inactivation was impacted by the commercial Laprotex™ fabric ($p < 0.001$) compared to the insignificant difference when using the PPW fabrics ($p = 0.260$). The fabric deposited with Al_2O_3 showed no significant difference ($p = 0.174$) between the fabric types, including the commercially available Laprotex™ fabric.

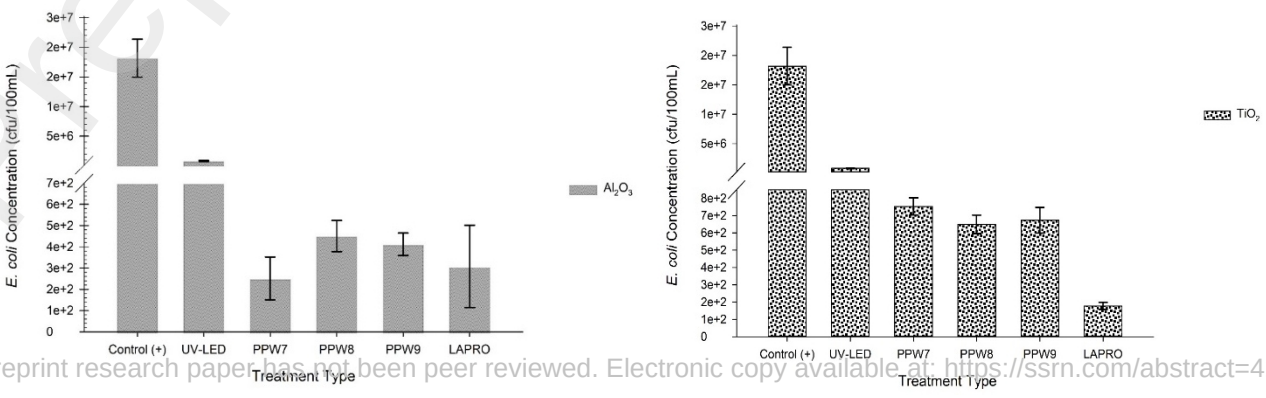

Figure 3: *E. coli* concentration, after exposure to UV-LED alone or UV-LED irradiating fabric deposited with photocatalysts (a) Al_2O_3 (n = 6) or (b) TiO_2 (n = 3). The represents the mean standard deviation for the experiment. Conditions: pH = 7, temperature = 25°C, λ = 255 nm, dose = 24.6 mJ/cm^2.

3.3. Stability of TiO_2 and Al_2O_3 thin film catalysts

The stability of the as synthesized TiO_2 and Al_2O_3 thin film catalysts was probed to determine the reusability of the coated meltblown nonwoven fabrics for larger scale use.

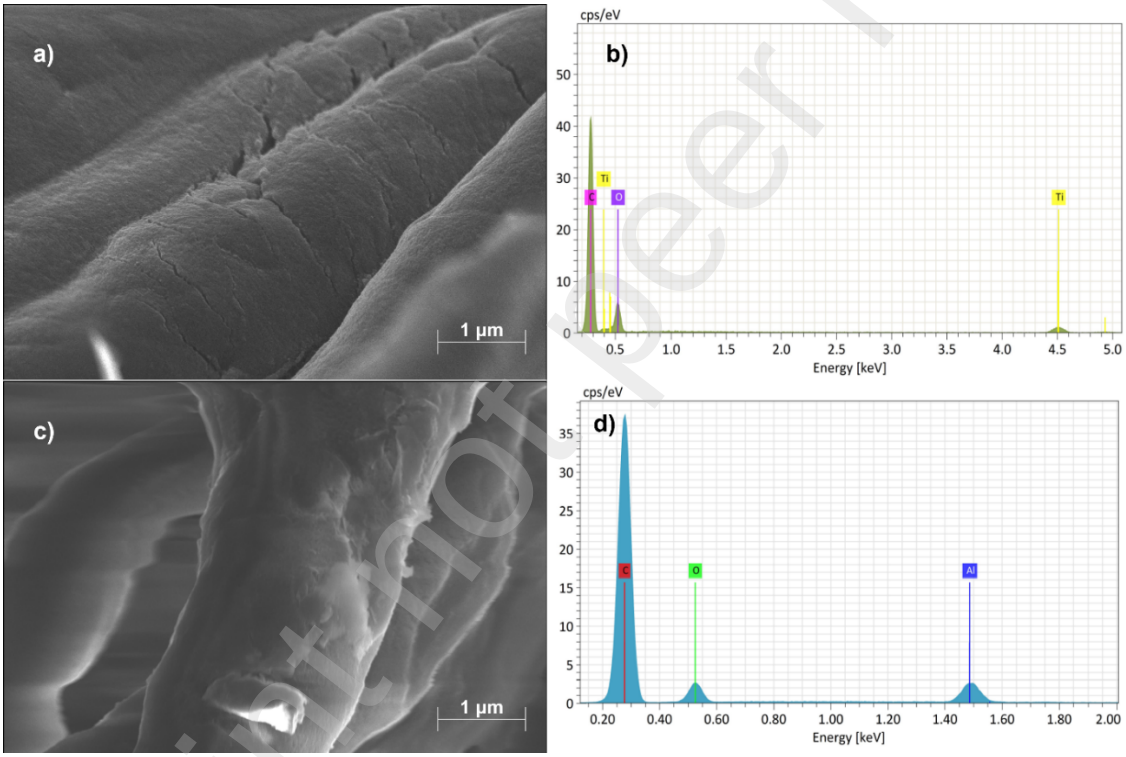

Figure 4: Structural morphology and composition of coated nonwovens after catalysis. a) SEM image of TiO_2 coated nonwoven fabric b) EDS spectrum of TiO_2 coated nonwoven fabric c) SEM image of Al_2O_3 coated nonwoven fabric d) EDS spectrum of Al_2O_3 coated nonwoven fabric.

Figure 4 details the morphology and elemental composition of the TiO_2 and Al_2O_3 coated nonwovens after catalysis. The overall film morphology remains relativity unchanged after catalysis. As evidenced by the EDS spectrum in Figure 4b and 4d, both the TiO_2 and Al_2O_3 films

remain relatively unchanged given the presence of the Ti and Al in the spectra. To further examine the change in catalyst films during catalysis, XPS was utilized to probe the changes in chemical structure of TiO_2 and Al_2O_3 and is shown in Figure 5.

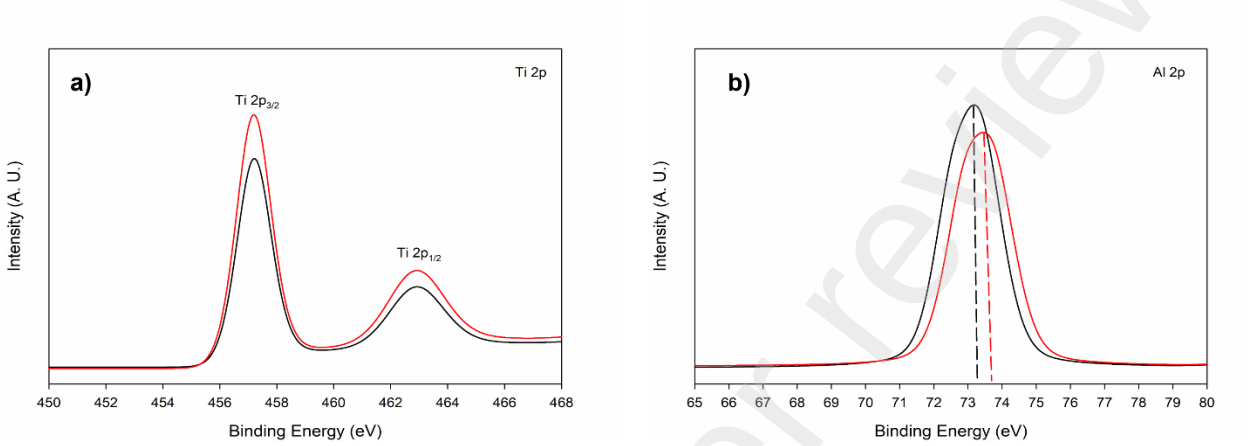

Figure 5: a) XPS spectrum for the Ti 2p electron before (black) and after (red) catalysis for TiO_2 coated nonwoven fabric b) XPS spectrum for the Al 2p electron before (black) and after (red) catalysis for Al_2O_3 coated nonwoven fabric.

The spectrum for the Ti 2p electron shown in Figure 5a shows no change in the characteristic peaks for Ti (IV) for the TiO_2 treated nonwoven fabric which suggests strong stability and reusability of the TiO_2 catalyst. The clearest change in the catalyst films was observed for the Al_2O_3 coated nonwoven fabric. The spectrum for the Al 2p electron shown in Figure 5b shows a clear shift in the characteristic peak for Al 2p after catalysis from 73.2 to 73.8 eV and suggests a partial change in oxidation state of Al after catalysis. Detailed atomic percentages as determined via XPS are shown in the Supporting Information (Table S3 and S4). This partial change in oxidation state suggests weaker stability for the Al_2O_3 films and is due to the presence of oxidized metal species given the oxidation condition during catalysis or the presence of new chemical states given the presence of N post catalysis as shown in Table S4.

4. Conclusion

Uniform TiO_2 and Al_2O_3 films were deposited on meltblown nonwovens via ALD and applied as a photocatalyst for the inactivation of *E. coli* in bulk water. It was found that the photocatalyst coated meltblown nonwovens outperformed the UV-LED light source utilized as evidenced by a near 4-fold increase in *E. coli* log inactivation for all fabrics tested with TiO_2 or Al_2O_3. In addition, it was found that for Al_2O_3 no significant difference in log inactivation was observed regardless of fabric type including the Laprotex™ fabric while for TiO_2, a significant difference between the Laprotex™ and PPW fabrics suggest that the bacterial inactivation was affected by the presence of the Laprotex™ fabric. Photocatalyst coated films were shown to have great stability given the minimal change in the structural morphology and elemental composition of the coated fabrics post catalysis. Minimal change in the Ti 2p XPS spectrum suggests TiO_2 films are completely intact post catalysis while the shift in the Al 2p XPS spectrum suggest a change in oxidation state likely due to the oxidation conditions during catalysis, and therefore less stability of the catalyst film. The utilization of ALD for the preparation of catalysts has strong potential for the development of sustainable, low environmental impact drinking water treatment technologies in the next few years. Furthermore, determination of the distinct hydroxyl radical groups produced in the photocatalytic process with allow for continued exploration of photocatalysts suitable for this application.

Acknowledgments

The authors thank Olubunmi Ayodele and Shobha Mantripragada from the Joint School of Nanoscience and Nanoengineering, University of North Carolina for providing XPS data. The Office of Research and Sponsored Programs at Wake Forest University provided generous financial support for the research detailed here within (CPG 1066).

References

[1] Odonkor, S. T.; Ampofo, J. K. Escherichia Coli as an Indicator of Bacteriological Quality of Water: An Overview. *Microbiology Research* **2013**, *4* (1), e2–e2. https://doi.org/10.4081/mr.2013.e2.

[2] Vietro, N. D.; Tursi, A.; Beneduci, A.; Chidichimo, F.; Milella, A.; Fracassi, F.; Chatzisymeon, E.; Chidichimo, G. Photocatalytic Inactivation of Escherichia Coli Bacteria in Water Using Low Pressure Plasma Deposited TiO2 Cellulose Fabric. *Photochem. Photobiol. Sci.* **2019**, *18* (9), 2248–2258. https://doi.org/10.1039/C9PP00050J.

[3] Park, J.; Kettleson, E.; An, W.-J.; Tang, Y. J.; Biswas, P. Inactivation of E. Coli in Water Using Photocatalytic, Nanostructured Films Synthesized by Aerosol Routes. *Catalysts* **2013**, *3* (1), 247–260. https://doi.org/10.3390/catal3010247.

[4] Ajiboye, T. O.; Babalola, S. O.; Onwudiwe, D. C. Photocatalytic Inactivation as a Method of Elimination of E. Coli from Drinking Water. *Applied Sciences* **2021**, *11* (3), 1313. https://doi.org/10.3390/app11031313.

[5] Khani, M.; Amin, N. A. S.; Hosseini, S. N.; Heidarrezaei, M. Kinetics Study of the Photocatalytic Inactivation of Escherichia Coli. *IJNBM* **2016**, *6* (3/4), 139. https://doi.org/10.1504/IJNBM.2016.086106.

[6] Ribeiro, M. A.; Cruz, J. M.; Montagnolli, R. N.; Bidoia, E. D.; Lopes, P. R. M. Photocatalytic and Photoelectrochemical Inactivation of Escherichia Coli and Staphylococcus Aureus. *Water Supply* **2014**, *15* (1), 107–113. https://doi.org/10.2166/ws.2014.084.

[7] Dunlop, P. S. M.; Ciavola, M.; Rizzo, L.; McDowell, D. A.; Byrne, J. A. Effect of Photocatalysis on the Transfer of Antibiotic Resistance Genes in Urban Wastewater. *Catalysis Today* **2015**, *240*, 55–60. https://doi.org/10.1016/j.cattod.2014.03.049.

[8] Friedman, N. D.; Temkin, E.; Carmeli, Y. The Negative Impact of Antibiotic Resistance. *Clin Microbiol Infect* **2016**, *22* (5), 416–422. https://doi.org/10.1016/j.cmi.2015.12.002.

[9] Benabbou, A. K.; Derriche, Z.; Felix, C.; Lejeune, P.; Guillard, C. Photocatalytic Inactivation of Escherischia Coli: Effect of Concentration of TiO2 and Microorganism, Nature, and Intensity of UV Irradiation. *Applied Catalysis B: Environmental* **2007**, *76* (3), 257–263. https://doi.org/10.1016/j.apcatb.2007.05.026.

[10] Aragon, A. G.; Kierulf-Vieira, W.; Łęcki, T.; Zarębska, K.; Widera-Kalinowska, J.; Skompska, M. Synthesis and Application of N-Doped TiO2/CdS/Poly(1,8-Diaminocarbazole) Composite for Photocatalytic Degradation of 4-Chlorophenol under Visible Light. *Electrochimica Acta* **2019**, *314*, 73–80. https://doi.org/10.1016/j.electacta.2019.05.060.

[11] Badhe, R. A.; Ansari, A.; Garje, S. S. Study of Optical Properties of TiO2 Nanoparticles and CdS@TiO2 Nanocomposites and Their Use for Photocatalytic Degradation of Rhodamine B under Natural Light Irradiation. *Bull Mater Sci* **2021**, *44* (1), 11. https://doi.org/10.1007/s12034-020-02313-1.

[12] Madkour, M.; Allam, O. G.; Abdel Nazeer, A.; Amin, M. O.; Al-Hetlani, E. CeO2-Based Nanoheterostructures with p–n and n–n Heterojunction Arrangements for Enhancing the Solar-Driven Photodegradation of Rhodamine 6G Dye. *J Mater Sci: Mater Electron* **2019**, *30* (11), 10857–10866. https://doi.org/10.1007/s10854-019-01429-3.

[13] He, Z.; Sun, C.; Yang, S.; Ding, Y.; He, H.; Wang, Z. Photocatalytic Degradation of Rhodamine B by Bi2WO6 with Electron Accepting Agent under Microwave Irradiation: Mechanism and Pathway. *Journal of Hazardous Materials* **2009**, *162* (2), 1477–1486. https://doi.org/10.1016/j.jhazmat.2008.06.047.

[14] Olagunju, M. O.; Zahran, E. M.; Reed, J. M.; Zeynaloo, E.; Shukla, D.; Cohn, J. L.; Surnar, B.; Dhar, S.; Bachas, L. G.; Knecht, M. R. Halide Effects in BiVO4/BiOX Heterostructures Decorated with Pd Nanoparticles for Photocatalytic Degradation of Rhodamine B as a Model Organic Pollutant. *ACS Appl. Nano Mater.* **2021**, *4* (3), 3262–3272. https://doi.org/10.1021/acsanm.1c00481.

[15] Bessekhouad, Y.; Chaoui, N.; Trzpit, M.; Ghazzal, N.; Robert, D.; Weber, J. V. UV–Vis versus Visible Degradation of Acid Orange II in a Coupled CdS/TiO2 Semiconductors Suspension. *Journal of Photochemistry and Photobiology A: Chemistry* **2006**, *183* (1), 218–224. https://doi.org/10.1016/j.jphotochem.2006.03.025.

[16] Choi, H.; Stathatos, E.; Dionysiou, D. D. Photocatalytic TiO2 Films and Membranes for the Development of Efficient Wastewater Treatment and Reuse Systems. *Desalination* **2007**, *202* (1), 199–206. https://doi.org/10.1016/j.desal.2005.12.055.

[17] Baghdadi, A. M.; Saddiq, A. A.; Aissa, A.; Algamal, Y.; Khalil, N. M. Structural Refinement and Antimicrobial Activity of Aluminum Oxide Nanoparticles. *Journal of the Ceramic Society of Japan* **2022**, *130* (3), 257–263. https://doi.org/10.2109/jcersj2.21140.

[18] Li, L.; Yu, P.; Li, Y.; Wu, X.; Li, W.; Cheng, X. A Facile Approach to Fabricating Antibacterial Textile with High Efficiency and Compact Process. *Advanced Materials Interfaces* **2021**, *8* (21), 2101197. https://doi.org/10.1002/admi.202101197.

[19] Popescu, M. C.; Ungureanu, C.; Buse, E.; Nastase, F.; Tucureanu, V.; Suchea, M.; Draga, S.; Popescu, M. A. Antibacterial Efficiency of Cellulose-Based Fibers Covered with ZnO and Al2O3 by Atomic Layer Deposition. *Applied Surface Science* **2019**, *481*, 1287–1298. https://doi.org/10.1016/j.apsusc.2019.03.268.

[20] Wang, Z.; Zhang, L.; Liu, Z.; Sang, L.; Yang, L.; Chen, Q. The Antibacterial Polyamide 6-ZnO Hierarchical Nanofibers Fabricated by Atomic Layer Deposition and Hydrothermal Growth. *Nanoscale Research Letters* **2017**, *12* (1), 421. https://doi.org/10.1186/s11671-017-2162-1.